The structure of polaronic electron cavities in lithium–ammonia solutions

2004 J. Phys.: Condens. Matter 16 5639

(http://iopscience.iop.org/0953-8984/16/32/001)

INSTITUTE OF PHYSICS PUBLISHING JOURNAL OF PHYSICS: CONDENSED MATTER

J. Phys.: Condens. Matter **16** (2004) 5639–5652 PII: S0953-8984(04)77324-5

The structure of polaronic electron cavities in lithium–ammonia solutions

Helen Thompson[1], Jonathan C Wasse[1], Neal T Skipper[1], Chris A Howard[1], Daniel T Bowron[2] and Alan K Soper[2]

[1] Department of Physics and Astronomy, University College London, Gower Street, London WC1E 6BT, UK
[2] ISIS Facility, Rutherford Appleton Laboratory, Chilton, Didcot, Oxfordshire OX11 0QX, UK

Received 2 March 2004
Published 30 July 2004
Online at stacks.iop.org/JPhysCM/16/5639
doi:10.1088/0953-8984/16/32/001

Abstract

Neutron diffraction has been used in conjunction with isotopic substitution of deuterium for hydrogen to study the structure of lithium–ammonia solutions, at concentrations spanning the metal–nonmetal transition. Detailed analysis and visualization of our experimental data has been carried out via iterative refinement of a three-dimensional molecular model, allowing us to obtain unique insight into the formation of polaronic electron cavities in the solutions. At low electron concentrations the solutions are nonmetallic, and the ammonia molecules are orientated around cavity centres to form Bjerrum-type defects. As the electron content is increased, the solutions become metallic, and we find evidence of percolation channels through the solvent. The dissociated electrons therefore play an active role in determining the structure of these solutions, and serve to disrupt the hydrogen bonding present in liquid ammonia.

1. Introduction

The dissolution of lithium in ammonia produces intensely coloured liquids in which the excess electrons are released into solution by solvation of the metal ions [1–3]. For a monovalent ion such as lithium, the concentration in mole per cent of electrons (MPE) is therefore equal to the concentration in mole per cent of metal (MPM). The remarkable properties of these electronic liquids have been well-documented, and include a metal–nonmetal transition, liquid–liquid phase separation, and very low density and viscosity.

If we focus briefly on the electronic species, we find that in dilute solutions of less than 2 mol% electrons (MPE), the electrons are localized, and have a pronounced tendency to form spin-paired bipolaronic species [4, 5]. Increasing the electron concentration above 4 MPE takes the solution through a metal–nonmetal transition. Cooling at this intermediate composition of ∼4 MPE leads to a striking liquid–liquid phase separation, in which the concentrated

(metallic) solution floats on the dilute (nonmetallic) phase. Above this concentration, the solutions become highly conducting and metallic. The excess electrons can then be viewed as being genuinely delocalized [4, 6], resulting in liquids of uncommonly low density and viscosity. Saturated (21 MPE) solutions of lithium in ammonia have a conductivity in excess of that for liquid mercury, and the lowest known freezing temperature for a metal.

Our neutron diffraction studies of liquid ammonia and lithium ammonia solutions have confirmed $Li(NH_3)_4^+$ as the dominant ionic species, and have shown that the hydrogen bonding present in liquid ammonia is progressively disrupted with increasing metal concentration by the presence of solvated ions and electrons [7]. Density measurements [3] and theoretical calculations [4, 5] predict that these electrons reside in weakly oriented solvent cavities of approximate radius 3 Å, forming continuous channels as the metal concentration is increased. This model is supported by interpretation of multinuclear magnetic resonance data [1], and by analysis of cavity distributions in neutron diffraction data [7]. However, experimental determination of the cavity structure itself must still be viewed as an outstanding challenge in the field.

In this paper we present new neutron diffraction data for nonmetallic lithium–ammonia solutions, which we compare with our previous data for pure ammonia and metallic solutions to provide a complete structural picture of this system. We have generated a three-dimensional model of lithium–ammonia solutions, constrained by our high-resolution neutron diffraction data via the empirical potential structure refinement (EPSR) technique [8–10]. This has allowed us to investigate the orientational correlations between solvent molecules, demonstrating the changeover from the hydrogen-bonded structure observed in the dilute regime to the solvated cation structure as the metal concentration is increased. Cavity-centred visualization has also enabled us to observe the active role played by the excess electrons in the structure of lithium–ammonia solutions. In fact, electron solvation should be viewed as an important factor in the decrease of hydrogen bonding with increasing metal concentration. Specifically, on raising the electron concentration from 2 to 8 MPE, a striking change in the orientation of ammonia molecules in the first electronic solvation shell is observed. This reorientation is likely to be caused by the fact that there are too few 'free' ammonia molecules available at this concentration to solvate the excess electrons [11]. This leads to the delocalization of the electrons and the formation of channels between the $Li–(NH_3)_4^+$ complexes, which give rise to the highly conducting metallic state.

2. Experimental details

2.1. Neutron diffraction

The technique of hydrogen/deuterium isotopic substitution [7, 12] has been used to investigate the structure of lithium–ammonia solutions at concentrations of 2, 3 and 4 MPE at a temperature of 230 K. These new data for the nonmetallic solutions are compared with previous data on pure liquid ammonia and metallic lithium–ammonia solutions at 8 and 21 MPE. For all concentrations of the lithium–ammonia solutions, three isotopically distinct samples were measured on the SANDALS diffractometer at the ISIS Facility of the Rutherford Appleton Laboratory. These comprised $Li–ND_3$, $Li–NH_3$ and a 50:50 mixture of $Li–ND_3$ and $Li–NH_3$ (50:50 being chosen here to maximize the scattering differences between the samples). For pure ammonia, the samples comprised ND_3, NH_3 and a 33:67 mixture of ND_3 and NH_3 (a so-called 'null scattering' mixture). In addition, first-order lithium difference experiments were carried out on the D4 diffractometer at the Institut Laue-Langevin and on the SANDALS diffractometer for the metallic solutions of concentrations 21 and 8 MPE respectively, the

samples here comprising ^{6}Li–ND_3 and ^{nat}Li–ND_3 [13, 14]. The samples were prepared using the procedure outlined in [7], in which a piece of lithium metal was mechanically cleaned, then weighed and loaded into the TiZr sample cell under an inert atmosphere (O_2 and H_2O less than 10 ppm). The cell lid and valve assembly was then sealed, removed from the glovebox and attached to a closed cycle refrigerator on the beamline. The cell was then attached to the gas panel via a 1/8 inch stainless steel capillary, and was evacuated to a pressure of less than 10^{-5} mbar. A known volume of ammonia gas was condensed directly onto the lithium metal at 230 K, to achieve the required concentration of metal in solution. For the mixed H/D samples, the NH_3 and ND_3 were mixed prior to condensation. The corrections for absorption, multiple scattering and background were implemented using the ATLAS suite of programs for the SANDALS data, and the analysis method detailed in [15] for the D4 data. The resulting datasets then give rise to the composite partial structure factors $S_{HH}(k)$, $S_{XH}(k)$, $S_{XX}(k)$ and $\Delta_{Li}(k)$, where H refers to the substituted hydrogen atoms, X refers to any nonsubstituted atoms and $\Delta_{Li}(k)$ is the lithium-centred first-order difference function [7]. The partial structure factor is related to the partial pair correlation function via

$$g_{\alpha\beta}(r) - 1 = \int_0^\infty \{k[S_{\alpha\beta}(k) - 1]\sin(kr)\,\mathrm{d}k\}/(2\pi^2\rho_0 r) \tag{1}$$

where k is the scattering vector, r is the position in real-space, and ρ_0 is the atomic number density of the sample.

Similarly, the total structure factor and the total pair correlation function are related by

$$F(k) = \frac{4\pi\rho_0}{k}\int_0^\infty rG(r)\sin(kr)\,\mathrm{d}r. \tag{2}$$

The average number of atoms of type β surrounding an atom of type α, between radii r_1 and r_2, is then calculated from

$$\bar{n}_\alpha^\beta = 4\pi\rho_0 c_\beta \int_{r_1}^{r_2} r^2 g_{\alpha\beta}(r)\,\mathrm{d}r \tag{3}$$

where ρ_0 is again the average atomic number density of the sample and c_β is the atomic fraction of type β.

A minimum noise Fourier transform [16] was used to produce the composite partial pair correlation functions presented here. This transform technique generates pair correlation functions which are as smooth as possible while still being consistent with the data. In this way we are able to produce radial distribution functions containing only real features which are not caused by truncation of the structure factor and/or noise within the structural data. Table 1 shows the relative contributions of the individual atom pairs within each function.

2.2. Empirical potential structure refinement (EPSR)

Empirical potential structure refinement (EPSR) [8–10] is a method which involves iterative refinement of an initial interatomic potential energy function, such that the resulting potential is able to produce the closest possible agreement between the simulated and measured site–site composite partial structure factors.

EPSR simulations were carried out on liquid ammonia and lithium–ammonia solutions spanning the metal–nonmetal transition at 2, 8 and 21 MPE at 230 K. The datasets used in the refinement procedure comprised the composite partial structure factors $S_{HH}(k)$, $S_{XH}(k)$ and $S_{XX}(k)$ for all the systems, and also included first-order lithium difference data for the metallic lithium–ammonia solutions at 8 and 21 MPE. The EPSR procedure uses a Monte Carlo simulation of molecules in a cubic box: the number of molecules at each concentration

Table 1. Weighting coefficients for the individual contributions to the X–X, X–H, H–H and lithium centred different functions for the lithium–ammonia solutions.

	0 MPM	2 MPM	3 MPM	4 MPM	8 MPM	21 MPM
H–H partial						
H–H	1.000	1.000	1.000	1.000	1.000	1.000
X–H partial						
N–H	1.000	1.004	1.006	1.009	1.018	1.057
Li–H	—	−0.004	−0.006	−0.009	−0.018	−0.057
X–X partial						
N–N	1.000	1.008	1.013	1.017	1.036	1.117
N–Li	—	−0.008	−0.013	−0.017	−0.036	−0.121
Li–Li	—	1.73E–05	3.99E–05	7.28E–05	0.0003	0.0033
Lithium difference						
Li–N	—	—	—	—	0.0036	0.010
Li–H	—	—	—	—	0.0077	0.021
Li–Li	—	—	—	—	−1.74E–06	−1.49E–05

Table 2. The number of molecules of each type and the cubic simulation cell sizes used in the EPSR simulations of liquid ammonia and lithium–ammonia solutions at 2, 8 and 21 MPE.

	Number of particles			
Sample (MPE)	NH_3	Li	e^-	Cell size (Å)
0	497	0	0	27.181
2	490	10	10	27.728
8	483	42	0	28.969
21	474	126	0	31.134

together with the simulation cell sizes are given in table 2. The ammonia molecule used was the 4-site OPLS model, initially with Lennard-Jones pair potentials for all atom–atom correlations and effective Coulomb charges taken from the literature [17, 18]. In the metallic solutions of 8 and 21 MPE, the electrons were not explicitly included since here the electrons are delocalized, although the density used reflected the volume expansion due to the accommodation of excess electrons in the solution. For the dilute solution of 2 MPE, the electrons were included as point charges and initially assigned a soft Lennard-Jones potential, to model their known localization in space via solvation by ammonia molecules [1–3]. The resulting empirical potential required to fit the neutron data is a perturbation added to the initial Lennard-Jones pair potentials: the amplitude of the perturbation is limited, such that the energy associated with the perturbation does not dominate the total energy of the simulation. The potential functions were constrained against all available datasets, combining data from both the D4 diffractometer and the SANDALS diffractometer in the case of the 21 MPE lithium–ammonia solution.

The EPSR analysis technique provides the opportunity to present a complete set of atom–atom partial pair correlation functions, which are consistent with the measured data. In addition, the EPSR procedure allows the implementation of a spherical harmonic expansion of the intermolecular structure in terms of polar coordinates r, θ and ϕ, in order to show the orientation correlations between molecules. Firstly a 'spatial density plot' can be obtained by holding molecule 1 fixed at the origin in a predefined orientation and averaging over all possible positions and orientations of the second molecule within a minimum and maximum

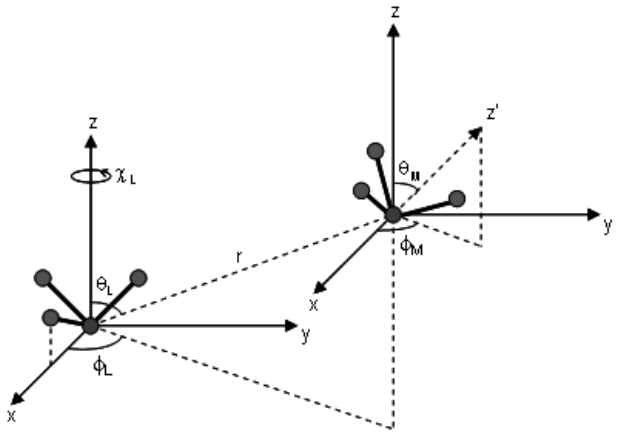

Figure 1. The coordinate system for the central reference ammonia molecule and a neighbouring ammonia molecule. The spatial density function is achieved by removing any dependence of the result on the orientation of molecule 2, and maps out the distribution of the centre of mass of the second molecule relative to the first. The orientational correlation function shows how the orientation of the second molecule is distributed as a function of r at a given (θ_L, ϕ_L, χ_L).

distance from the first molecule, allowing θ_L and ϕ_L to vary. Secondly, we are able to probe the most probable dipole orientations of the second molecule relative to the first for each of the lobes appearing in the spatial density plot, again by fixing molecule 1 at the origin in its predefined orientation, but this time holding the direction of the centre of molecule 2 from the centre of molecule 1 fixed and by setting θ_L, ϕ_L (the direction of the centre of the second molecule from the first) at the angle of interest, and allowing θ_M and ϕ_M (the orientation of the second molecule within its own coordinate frame) to vary. The angles θ and ϕ are defined relative to the z-axis (dipole moment) of the ammonia molecule and the x–z plane (in which the first intramolecular N–H bond lies) respectively, as shown in figure 1.

Such an analysis yields the orientational molecular distributions of ammonia molecules relative to a central ammonia molecule, and the dipolar molecule–molecule orientations. This allows the directionality of the hydrogen bonding to be investigated. In addition, we have searched the resulting 3D configurations for polaronic cavities within the solvent using the method described in section 3.2, and have then measured the angular distribution of the ammonia molecules that solvate these cavities.

3. Results and discussion

The total structure factors for the deuterated samples together with the minimum noise fits and the corresponding pair correlation functions for the 2, 3, and 4 MPE lithium–ammonia solutions are presented in figure 2(a), together with previous data on liquid ammonia for comparison. The minimum noise fits show excellent agreement with the measured data, and therefore give confidence in the data analysis techniques used. Upon addition of lithium metal to ammonia, a decrease in the position of the principal peak in $F(k)$ is observed, from 2.08(2) Å^{-1} in liquid ammonia, to 2.07(2) Å^{-1} in the dilute solutions (2, 3 and 4 MPE). This can be compared with principal peak positions of 2.01(2) and 1.85(2) Å^{-1} in the 8 and 21 MPE solutions respectively.

Figures 2(b)–(d) show the composite partial structure factors, $S_{HH}(k)$, $S_{XH}(k)$ and $S_{XX}(k)$, together with the corresponding composite partial pair correlation functions. From these functions it can be seen that all intramolecular distances within the ammonia molecules are

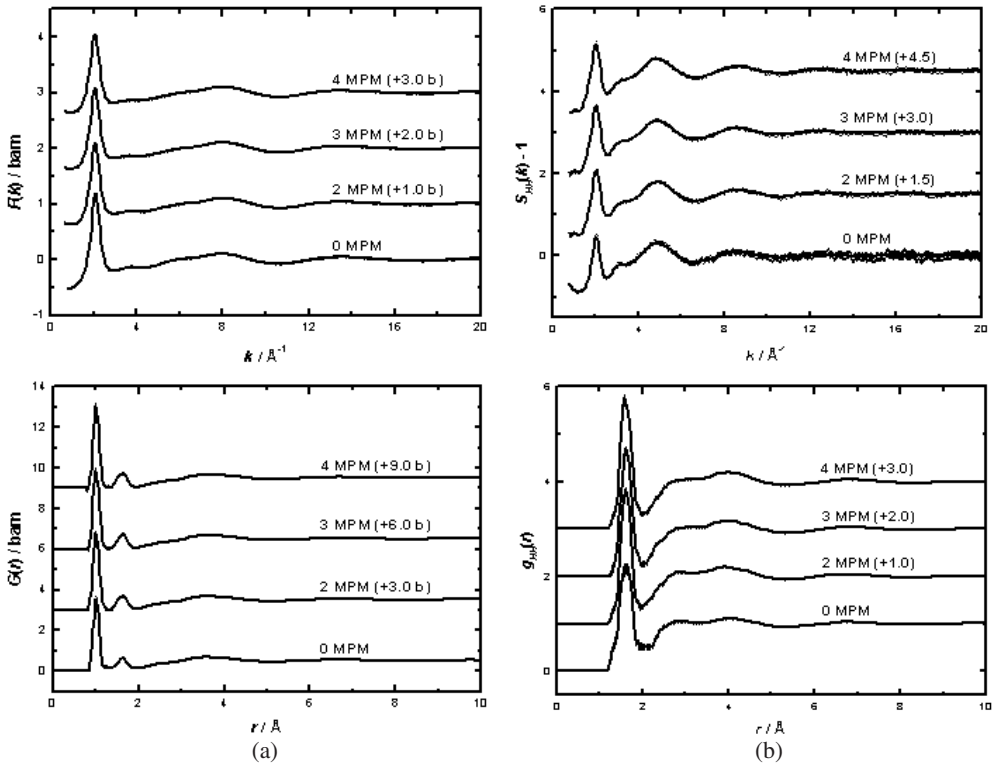

(a) (b)

Figure 2. (a) Total structure factors (error bars) and minimum noise fit (solid curve) and the total pair correlation functions for the deuterated samples; (b)–(d) H–H, X–H and X–X partial structure factors (error bars) and minimum noise fit (solid curve) and the corresponding partial pair correlation functions.

unaffected by the presence of the lithium cations and excess electrons. Furthermore, the principal peak position in all three of the partial structure factors decreases with metal content, in accordance with the total structure factors. This effect reflects the overall reduction in solution density, and leads to corresponding peak shifts in the high-r region of the partial pair correlation functions.

In the context of hydrogen bonding, the key functions are the X–H partial structure factors and radial distributions. In liquid ammonia, integration of the shoulder at ∼2.4 Å yields an average of 2.0 ± 0.5 hydrogen bonds per nitrogen atom. Addition of lithium metal causes a large decrease in the number of hydrogen bonds per nitrogen atom, to 1.4 ± 0.2, 1.1 ± 0.2 and 0.95 ± 0.2 bonds per nitrogen atom in the 2, 3, and 4 MPE solutions respectively. This can be compared with 0.7 ± 0.2 and 0.0 hydrogen bonds in the 8 and 21 MPE solutions. These numbers were obtained by direct integration of the hydrogen-bonded shoulder, up to a distance of ∼2.65 Å, i.e. the point of inflexion in the N–H radial distribution function. This disruption to the hydrogen bonding in solutions of intermediate concentration is greater than that expected if ionic solvation alone were taken into account, suggesting that the solvation of excess electrons does indeed have a role to play in determining the structure of the solutions. This will be explored in detail in section 3.2.

EPSR simulations were performed on liquid ammonia and lithium–ammonia solutions at 2, 8 and 21 MPE. The simulated partial structure factors arising from the final EPSR configurations are presented in figure 3, together with the experimental data. The discrepancy between the

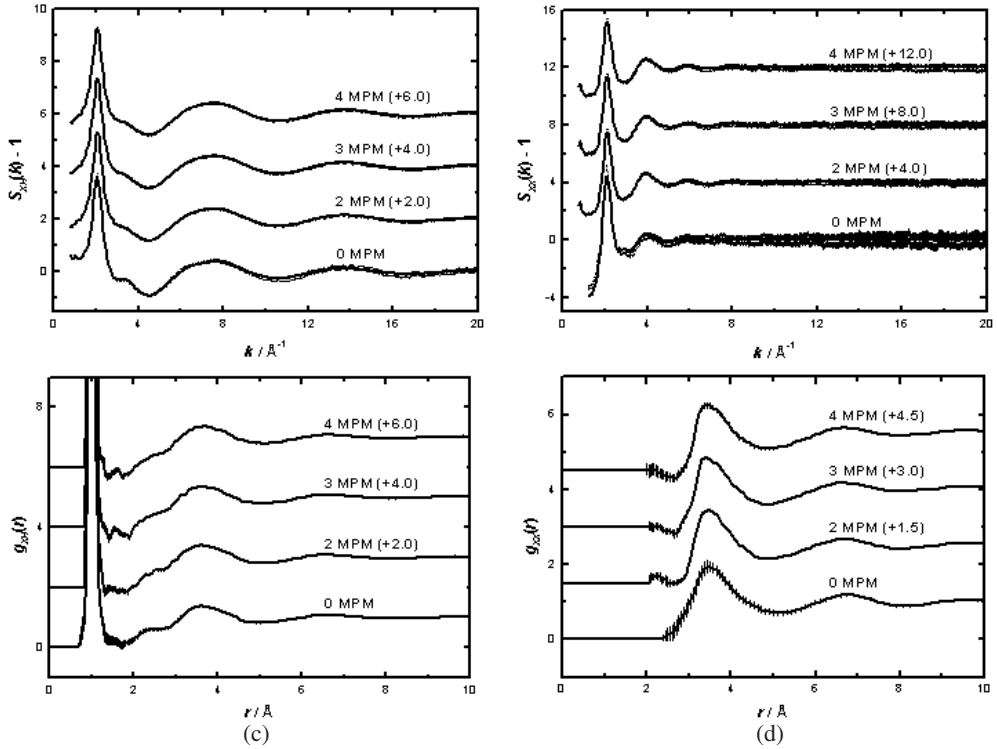

(c) (d)

Figure 2. (Continued.)

EPSR fit and the measured structure factors at the lower k-values is due to the residual inelastic scattering from hydrogen atoms which is difficult to remove completely from the neutron data. The neutron data were truncated at ∼0.7–1.0 Å, as this was the limit of reliability of the SANDALS instrument. It should be noted that the small peaks occurring at low k in the simulated partial structure factors are not real features, since the simulation cell sizes used were typically ∼27–28 Å. The empirical potential is truncated at a half of the box size, so the reliability of the k-space simulation data extends down to $2\pi/14 \sim 0.5$ Å^{-1}. No claims have been made on the basis of the low-k features: here we are interested in intermolecular correlations at distances below 6 Å.

Representative interatomic radial distribution functions for the 2 MPE lithium–ammonia solution are shown in figure 4. The Li–N and Li–H correlations confirm that lithium is strongly solvated, with Li–$(NH_3)_4^+$ forming the dominant cationic structural motif [13, 14]. Orientationally averaged information on the hydrogen bonding is contained within the N–H and H–H radial distribution functions. Integration of the arrowed shoulder at around 2.4 Å in the N–H partial pair correlation function reveals ∼1.4 hydrogen bonds per nitrogen atom in the 2 MPE solution. The equivalent integration of the N–H partial pair correlation function for the 0, 8 and 21 MPE lithium–ammonia solutions yields 2.0, 0.7 and 0.0 hydrogen bonds respectively per nitrogen atom, numbers which are consistent with those obtained experimentally [7].

3.1. Hydrogen bonding directionality

The resulting 3D molecular configuration which is consistent with the measured data can then be used to probe for the first time the subtle spatial arrangements and molecular orientations that

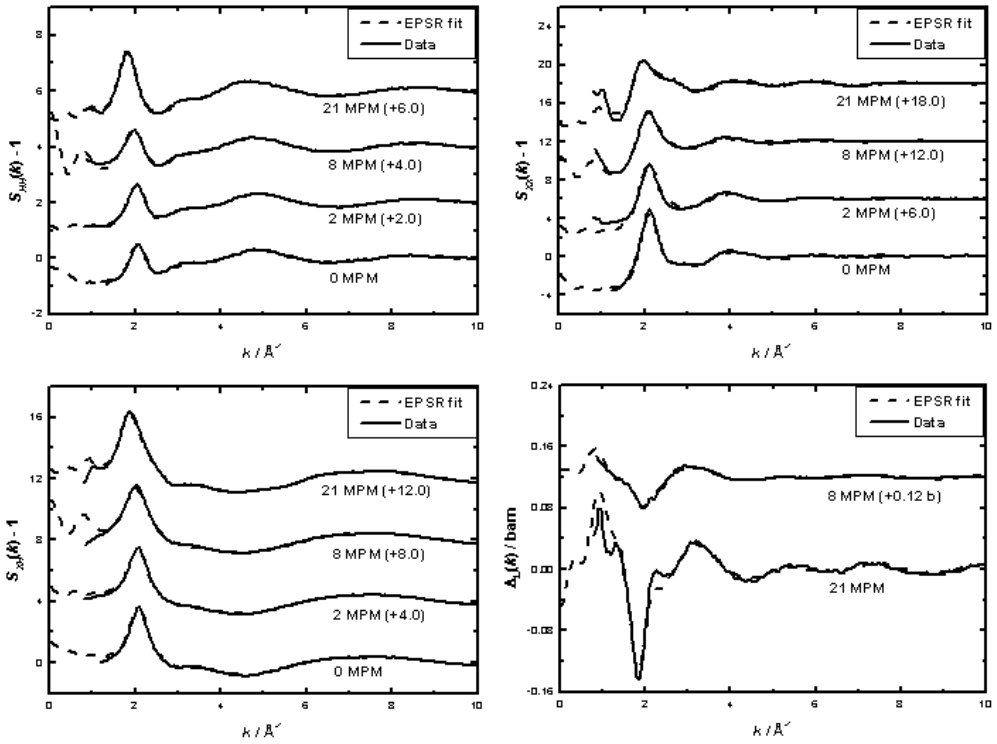

Figure 3. Comparison of the EPSR fits to the measured composite partial structure factors for the liquid ammonia and lithium–ammonia solutions at 2, 8 and 21 MPE. (a) H–H and X–H, (b) X–X and lithium centred difference function $\Delta_{\mathrm{Li}}(k)$ [7].

accompany this breakdown in hydrogen bonding, as the solutions expand and become metallic. The three-dimensional spatial distribution of nitrogen atoms in the first N–N shell is presented as a function of electron concentration in figure 5. The orientation of the central reference molecule is fixed, and the surfaces shown enclose regions of maximum spatial density. The surface contour level was selected in the present case to include 20% of all the ammonia molecules within 5 Å of the central molecule. Note that in a sufficiently disordered system, a plot of 100% of the molecules would not demonstrate the preferential angular positions/dipole directions, and would yield a distribution which would appear isotropic.

In pure ammonia, the directions in which hydrogen bonding occurs can clearly be seen, with three acceptor lobes positioned above the hydrogen atoms on the central molecule, and a trefoil-shaped donor lobe below. In total, six approach directions are observed, reminiscent of the six hydrogen bonds that are formed in solid ammonia [19–21]. The dipole orientations of the neighbouring ammonia molecules are presented in figure 6, showing the tendency for the molecules in the acceptor lobes to direct their dipole moment away from the central reference molecule, and the dipole moments of the molecules in the donor lobe to be towards the central ammonia molecule in the toroidal shape shown.

In the 21 MPE lithium–ammonia solution, no acceptor lobes at $(\theta_{\mathrm{L}}, \phi_{\mathrm{L}}) = (60, 120)$ are visible. At this threshold, the density surface is inverted from that in pure ammonia, as the molecules approach face to face via Li–$(NH_3)_4^+$ complexes, as shown in figure 7. Furthermore, the dipole moments of the band below the central ammonia (figure 6) are directed away from

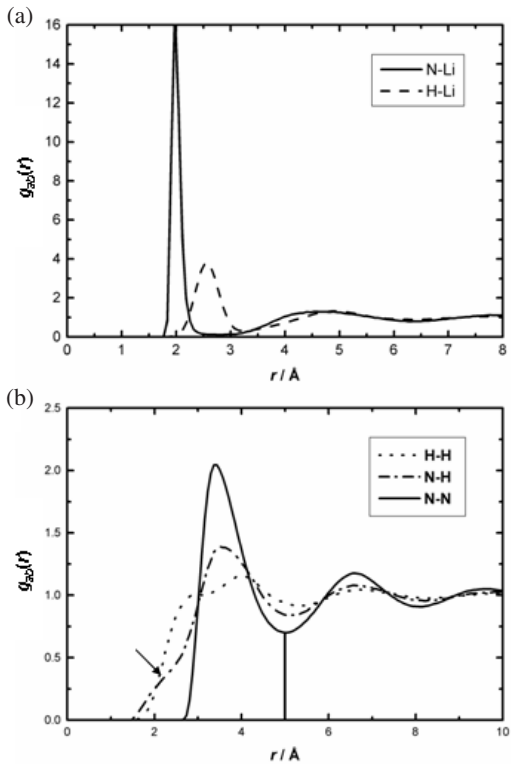

Figure 4. (a) N–Li and H–Li radial distribution functions showing the ionic solvation shell of ∼4.0 ammonia molecules, and (b) representative interatomic solvent–solvent radial distribution functions for the 2 MPE lithium–ammonia solution. Note that the first N–N shell extending to ∼5 Å contains a significant contribution from hydrogen-bonded solvent molecules, illustrated by the arrowed hydrogen-bonded shoulder at ∼2.2 in the N–H radial distribution function and the shoulder at 2.7 Å in the H–H radial distribution function.

the molecule, and the dipole moments of the ammonia molecules at $(\theta_L, \phi_L) = (60, 120)$ are now directed *towards* the central reference molecule. This confirms the lack of hydrogen bonding in a saturated solution which is comprised solely of solvated ions and delocalized excess electrons.

For the 2 and 8 MPE lithium–ammonia solutions, it is apparent that some degree of hydrogen bonding is still present. The dipole moments of the lobe at $(\theta_L, \phi_L) = (60, 120)$, shown in figure 6, are seen to direct themselves away from the hydrogen atoms on the central molecule, as in pure ammonia. The dipole moments of the lobe at $(\theta_L, \phi_L) = (180, 0)$ below the central molecule in the 8 MPE solution, however, consist of some moments directed upwards towards the nitrogen atom of the central molecule, in the toroidal shape characteristic of hydrogen bonding as in pure ammonia, and some moments pointing directly away from the central ammonia molecule, as in the saturated solution. The sequence of nearest neighbour N–N distributions and dipole orientations from 0, through 2 MPE and 8 to 21 MPE thus enables us to differentiate between two populations of ammonia molecules: those that are hydrogen bonded and those responsible for ion solvation. It is primarily the balance between hydrogen bonding in the solvent and ionic solvation which drives the structure of the lithium–ammonia solution across the metal–nonmetal transition.

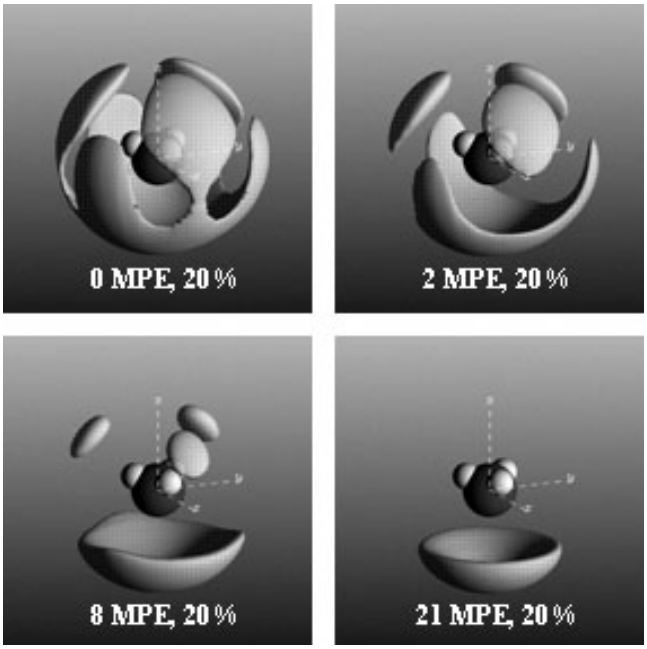

Figure 5. Spatial density plots of the first N–N shell for liquid ammonia and 2, 8 and 21 MPE lithium–ammonia solutions. The grey-shaded regions show the most likely angular positions of nearest neighbour nitrogen atoms around a central ammonia molecule.

3.2. Polaronic cavity formation and electron solvation

With increasing metal content, the degree to which ionic solvation influences the structure increases relative to that of hydrogen bonding. However, it is apparent that an additional mechanism is responsible for the hydrogen bonding disruption with metal concentration. The graph in figure 8 shows the calculated number of hydrogen bonds per nitrogen atom, assuming that the disruption to hydrogen bonding is solely due to tetrahedral solvation of the cations, together with the measured number of hydrogen bonds per nitrogen atom. The calculated number of hydrogen bonds per nitrogen atom was carried out as follows:

$$\bar{n}_{\mathrm{N-H}} = \left(1 - \frac{n_{\mathrm{ion-bound}}}{n_{\mathrm{total}}}\right) \times 2.0$$

where $\bar{n}_{\mathrm{N-H}}$ is the estimated number of hydrogen bonds per nitrogen atom, $n_{\mathrm{ion-bound}}$ is the number of ammonia molecules bound to a cation, n_{total} is the total number of ammonia molecules, and the multiplicative factor of 2.0 is the average number of hydrogen bonds per nitrogen atom in pure ammonia. It is clear from the graph that the disruption to the hydrogen bonding is significantly greater than that expected if ionic solvation were the only factor responsible.

We propose that the additional decrease in hydrogen bonding is caused by the accommodation of the dissociated electrons within the solution. Magnetic resonance measurements and *ab initio* simulations have provided evidence that an isolated excess electron occupies a solvent cavity of approximate radius 3 Å [1, 4, 5]. In order to investigate the direct influence of the electrons on the solvent structure, the molecular configurations obtained via EPSR have been analysed for voids of $\sim$5 Å diameter such that their distribution may be plotted relative to the ammonia molecules. This was carried out in the following way: points were

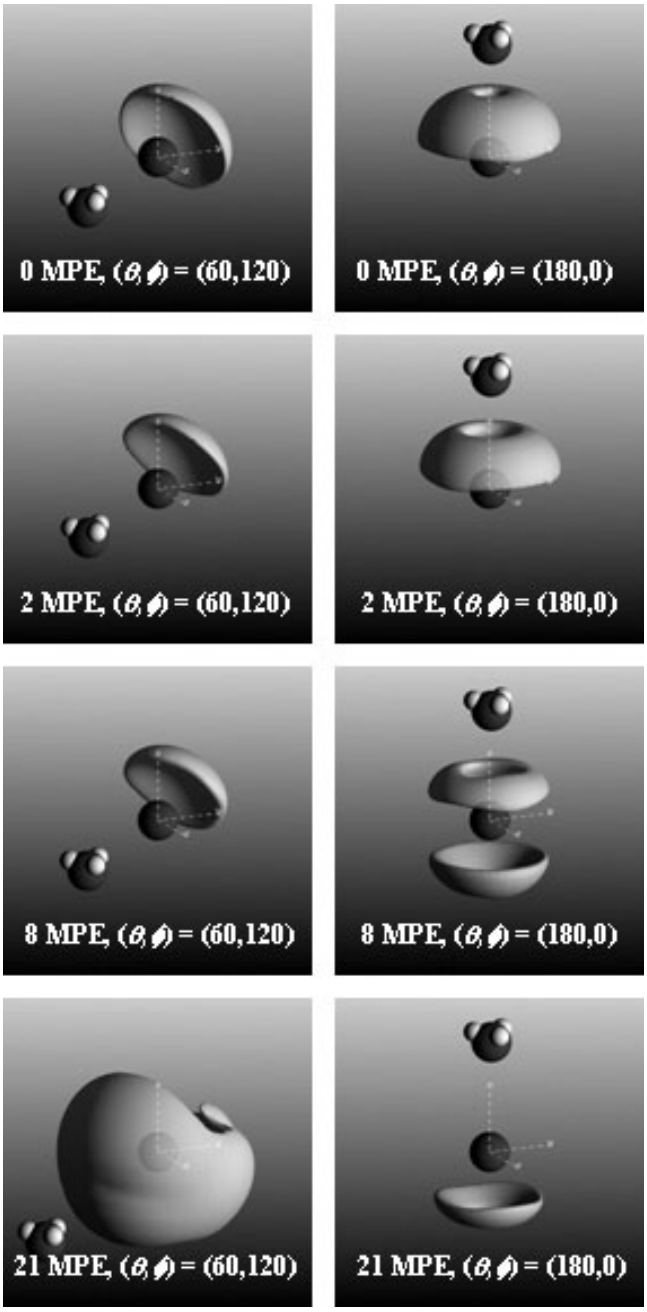

Figure 6. Dipole orientations of the ammonia molecules in the first N–N shell in liquid ammonia and 2, 8 and 21 MPE lithium–ammonia solutions: column 1 refers to $(\theta_L, \phi_L) = (60, 120)$, column 2 refers to $(\theta_L, \phi_L) = (180, 0)$. The grey-shaded regions represent the most likely directions of the dipole moment of the ammonia molecule; the fraction of ammonia molecules shown is 30%.

chosen on a regular grid, approximately every 1.5 Å in the x, y and z directions. A void was recorded for each grid point for which no atomic centres were found within a sphere of radius 2.5 Å defined around that point [7]. The slightly smaller radius of 2.5 Å was used here to

Figure 7. Orientational distribution of the first and second solvation shells of ammonia around a central lithium cation at 8 MPE. The tetrahedral set of grey spheres represents the first solvation shell, the grey-shaded region the second solvation shell.

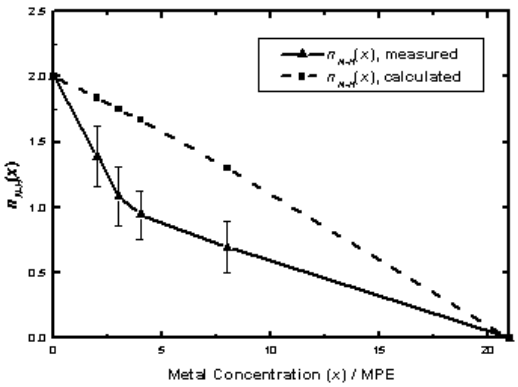

Figure 8. Graph showing the measured number of hydrogen bonds per nitrogen atom (triangles, solid curve) and the calculated average number of hydrogen bonds per nitrogen atom if ionic solvation were the sole mechanism responsible for hydrogen bonding disruption (squares, dashed curve) versus metal concentration.

allow for the fact that a void may not be exactly spherical: a search for 3 Å spheres containing no atomic centres would immediately discount several of the solvent cavities appearing in the EPSR configuration. This analysis was performed over at least 150 iterations of the molecular configuration at each metal concentration.

Figure 9 shows the angular distribution of electronic voids around a central ammonia molecule. Radial distribution functions (NH_3–void) alone show only a one-dimensional average of the distribution of ammonia molecules around a void, and it is difficult to visualize the orientation of these ammonia molecules relative to the void. Spatial density functions provide fresh insight into the reorientation of the ammonia molecules as the concentration of electrons and ions increases, and are able to shed more light on the mechanism of electron solvation. Note that, even in the case of pure ammonia, a small number of voids are evident

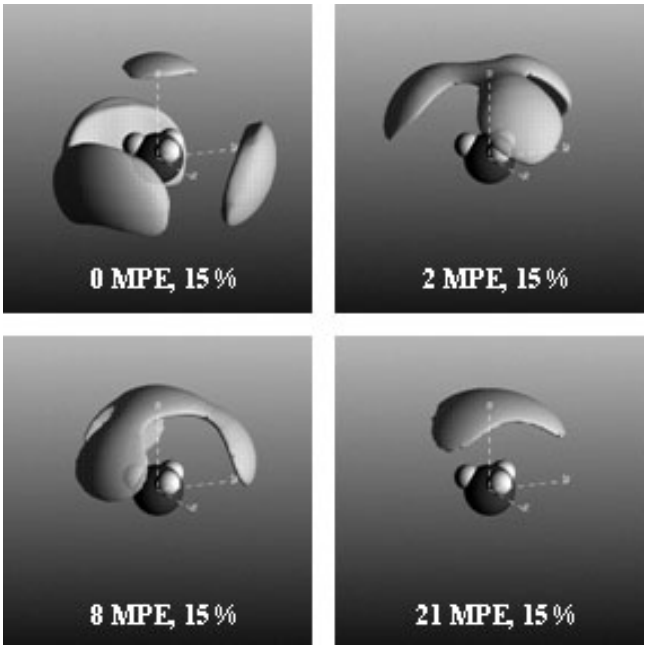

Figure 9. Angular distribution of voids (grey-shaded regions) caused by accommodation of excess electrons relative to the ammonia molecules. The fraction of voids plotted is 15%.

in between the hydrogen-bonded lobes shown in figure 4, despite the fact that there is no requirement to accommodate any excess electrons.

In the 2 MPE solution, the solvent structure around the electronic cavities is clearly very different: ammonia molecules in the first coordination shell direct one hydrogen atom per molecule towards the centre of the void, forming a Bjerrum-type defect [22]. At this metal concentration, the electrons are fully solvated, and the first solvation shell comprises $\sim 9 \pm 2$ ammonia molecules, in agreement with the number predicted by path-integral Monte Carlo and molecular dynamics simulations and magnetic resonance studies [1, 23].

Upon increasing the metal concentration from 2 to 8 MPE, it can be seen that the orientation of the ammonia molecules around the polaronic cavities changes dramatically, such that two hydrogen atoms per ammonia molecule are now directed towards the void. At 8 MPE, the number of 'free' ammonia molecules per electron is only $\sim$7.5. It has been suggested that this number is too few to be able to solvate the electron completely [11] since at this concentration the lithium–ammonia solution is truly metallic with an electrical conductivity of 1500 Ω^{-1} cm^{-1}. Therefore, it is likely that the observed reorientation of the ammonia molecules compensates for the lack of free ammonia molecules available for electron solvation.

Finally, at saturation, all the ammonia molecules have become incorporated into the first cation solvation shells. At this concentration we find that percolation channels form between the Li–$(NH_3)_4^+$ complexes, and the dipole moments of the ammonia molecules are directed towards these electron channels, as shown in figure 9.

4. Conclusions

In summary, via a full interpretation of experimental data in terms of coordination numbers and 3D modelling, we have been able to observe the active role of the excess electrons on

the structure of lithium–ammonia solutions. The visualization technique employed here has revealed that electron solvation is the additional factor in determining the decrease in hydrogen bonding with metal concentration, further to that caused by ionic solvation. In addition, the EPSR model provides new insight which is crucial to our understanding of the interplay between hydrogen bonding and electron localization/delocalization across the metal–nonmetal transition. Upon increasing the electron concentration from 2 to 8 MPE, we observe a striking change in the orientation of ammonia molecules in the first electronic solvation shell. This reorientation is likely to be caused by the fact that there are too few free ammonia molecules available at this concentration to solvate the excess electrons. This leads to the delocalization of the electrons and the formation of channels between the Li–$(NH_3)_4^+$ complexes, which give rise to the highly conducting metallic state.

Acknowledgments

We would like to acknowledge the assistance of John Dreyer, John Bones, Chris Goodway and Rob Done (ISIS Facility), and Henry Fischer and Pierre Palleau (ILL), and to thank Peter Edwards for many useful discussions. We are grateful for financial support from the ISIS Neutron Scattering Facility and UK EPSRC.

References

[1] Edwards P P 1984 *J. Phys. Chem.* **88** 3772
[2] Edwards P P 1982 *Adv. Inorg. Chem.* R **25** 135
[3] Thompson J C 1976 *Electrons in Liquid Ammonia* (Oxford: Clarendon)
[4] Deng Z, Martyna G J and Klein M L 1993 *Phys. Rev. Lett.* **71** 267
[5] Deng Z, Martyna G J and Klein M L 1992 *Phys. Rev. Lett.* **68** 2496
[6] Kohanoff J, Buda F, Parrinello M and Klein M L 1994 *Phys. Rev. Lett.* **73** 3133
[7] Thompson H, Wasse J C, Skipper N T, Hayama S, Bowron D T and Soper A K 2003 *J. Am. Chem. Soc.* **125** 2572
[8] Soper A K 1996 *Chem. Phys.* **202** 295
[9] Bowron D T, Finney J L and Soper A K 1998 *J. Phys. Chem.* B **102** 3551
[10] Soper A K 2001 *Mol. Phys.* **99** 1503
[11] Hayama S, Wasse J C, Skipper N T and Thompson H 2002 *J. Chem. Phys.* **116** 2991
[12] Soper A K, Howells W and Hannon A C 1989 ATLAS-analysis of time-of-flight diffraction data from liquid and amorphous samples *Rutherford Appleton Laboratory Report* RAL-89-046
[13] Wasse J C, Hayama S, Skipper N T and Fischer H E 2000 *Phys. Rev.* B **61** 11993
[14] Wasse J C, Hayama S, Skipper N T, Benmore C J and Soper A K 2000 *J. Chem. Phys.* **112** 16
[15] Salmon P S, Xin S and Fischer H E 1998 *Phys. Rev.* B **58** 6115
[16] Soper A K, Andreani C and Nardone M 1993 *Phys. Rev.* E **47** 2598
[17] Rizzo R C and Jorgensen W L 1999 *J. Am. Chem. Soc.* **121** 4827
[18] Chandrasekhar J, Spellmeyer D and Jorgensen W L 1984 *J. Am. Chem. Soc.* **106** 903
[19] Reed J W and Harris P M 1961 *J. Chem. Phys.* **35** 1730
[20] Hewat A W and Riekel C 1979 *Acta Crystallogr.* A **35** 569
[21] Olovsson I and Templeton D H 1959 *Acta Crystallogr.* **12** 832
[22] Catterall R and Mott N F 1969 *Adv. Phys.* **18** 665
[23] Marchi M, Sprik M and Klein M L 1988 *Faraday Discuss. Chem. Soc.* **85** 373